Optics and Laser Technology 119 (2019) 105675

Contents lists available at ScienceDirect

Optics and Laser Technology

journal homepage: www.elsevier.com/locate/optlastec

Full length article

Effect of thickness non-uniformity of large-area grating metal film on grating diffraction wavefront

Xiaotao Mi*, Shanwen Zhang, Xiangdong Qi, Hongzhu Yu, Jingxuan Zhou, Sibo Jiang

Grating Technology Laboratory, Changchun Institute of Optics and Fine Mechanics and Physics, Chinese Academy of Sciences, Changchun, Jilin 130033, China

HIGHLIGHTS

- The effect of film thickness non-uniformity on the grating wavefront is studied.
- The effect of relevant factors on the film thickness uniformity is analyzed.
- The values of the factors affecting the film thickness uniformity are determined.
- The wavefront quality increases with improvement in the film thickness uniformity.

ARTICLE INFO

Keywords:
Gratings
Metal film thickness non-uniformity
Grating diffraction wavefront error

ABSTRACT

As the grating area increases, the non-uniformity of the metal film thickness becomes one of the main factors affecting both the grating surface error and the wavefront of the grating diffraction order. We study the theoretical model of the relationship between the metal film thickness non-uniformity and the grating diffraction wavefront error, analyze the effects of the relevant factors on the thickness of the metal films, and determine the values of these factors using theoretical and experimental methods. We also perform a ruling experiment to verify that the wavefront quality of the grating increases with improvement in the film thickness uniformity.

1. Introduction

Operation at high spectral orders and high diffraction angles gives echelles the advantages of high dispersion, broad spectrum operation and high spectrum resolution [1–3]. Large-size echelles, which offer stronger concentrating powers and higher resolutions, have become core components of spectrometers for applications including astronomical telescopes and elemental analysis [4–6]. Because of the deep grooves and strict shapes that are required, these echelles are produced by the mechanical ruling method [7–10].

As the grating area increases, the difficulty involved in fabricating both the blank and the metal films will also increase, the grating ruling time will increase, and the effects of environmental changes on the grating will become more obvious. Processing of the grating substrate is generally completed by professional manufacturers and the effects of the environment on the grating will be detailed in a subsequent paper. We assume that the substrate plane is flat and does not affect the wavefront of the grating. Therefore, the quality of the metal film is the main research focus of the work described in this paper.

To date, research on large-area metal films has mainly concentrated on the aluminum mirrors used in large-scale optical systems, and the thickness of the aluminum films used in these mirrors is generally controlled to a precision of several hundred nanometers. However, the metal films that are used for ruling of echelles require film thicknesses of several micrometers or even tens of micrometers [11–14]. The current ruling engines that are capable of ruling large-area echelles include the MIT-C engine and the CIOMP-6 engine. The MIT–C engine can rule blanks with dimensions ranging up to 450 mm × 650 mm × 125 mm, but there is no relevant literature that describes the ruling films for large gratings fabricated by the MIT-C engine [15,16]. We have now summarized a set of film deposition processes for the ruling of echelles and have ruled high-quality echelles with dimensions of less than 150 mm × 150 mm [17–19].

In this study, we present a systematic study of the relationship between the non-uniformity of the metal film thickness and the resulting grating diffraction wavefront error with a specific focus on improving the diffraction wavefront quality of large-size echelles. First, we establish a mathematical model of the relationship between the blank surface shape error and the grating diffraction wavefront, and derive the non-uniformity error requirements for these metal films. We then

* Corresponding author.
E-mail address: mixiaotao_ciomp@126.com (X. Mi).

https://doi.org/10.1016/j.optlastec.2019.105675
Received 12 December 2018; Received in revised form 12 May 2019; Accepted 30 June 2019
Available online 06 July 2019
0030-3992/

analyze the effects of the relevant factors on the thicknesses of the metal films and the effects of metal film thickness non-uniformity on the grating diffraction wavefront using both simulations and experiments. Finally, we reduce the thickness non-uniformity of the large-area thick metal films, which leads to greatly improved wavefront quality for the large-size echelles.

2. Theory

The accuracy of the ruling engine operation and the grating blank surface error are the two main factors that affect the grating groove position error. This groove position error will then affect the grating performance. Non-uniformity in the thickness of large-area thick metal films will lead directly to errors in the surface shape of the blank, which in turn affects the grating wavefront error. To ease the analysis of the errors, we make two assumptions: (1) equidistant ruling occurs on the ideal plane, i.e., the grating groove is in the ideal position without the influence of the grating blank surface error; (2) the distance from a point on the metal film to the ideal ruling plane before the grating is ruled is the same as the distance from the corresponding point on the actual groove shape to the ideal groove shape after the grating is ruled. Because of the surface error of the grating blank, the grooves are not equidistant on the real surface and the angles of incidence would technically have to be modified for the local grating. However, for the typical small surface errors that occur in optics, the angular deviation of the entire grating plane is extremely low and can thus be neglected. Based on the above assumptions and analysis, for simplicity, we ignore the groove shape detail of the grating, and the grating groove errors will produce the optical path difference shown in Fig. 1. In the main section of the grating, monochromatic light with wavelength λ is incident on the grating surface to be measured, the angle of incidence on the grating is denoted by α, and the grating diffraction angle is denoted by β. The grating groove direction is the y direction (which is perpendicular to the plane of the paper), the depth difference between a single point i on the section of the grating and the ideal surface of the grating is denoted by $p(x_i, y_i)$, and the optical path difference produced by this depth difference is given as

$$\delta_{bi} = \delta_{bi1} + \delta_{bi2} = p(x_i, y_i)(\cos\alpha + \cos\beta) \quad (1)$$

The grating diffraction equation is given by:

$$d\cdot(\sin\alpha + \sin\beta_m) = m\cdot\lambda \quad (2)$$

where d is the grating constant, β_m is the mth-order diffraction angle, m is the diffraction order and λ is the incident light wavelength.

Eqs. (1) and (2) can be combined to allow the diffraction wavefront error of the grating, which is caused by the depth difference, to be written as

$$\Delta(m) = p(x, y)\cdot(\cos\alpha + \cos\beta_m) \quad (3)$$

where $p(x,y)$ is the surface error of the entire grating plane, and β_m is the mth-order diffraction angle and can be calculated using Eq. (2).

If the grating wavefront difference is caused solely by the surface error in the grating blank, the shape error requirements of the blank can be derived from Eq. (3) based on the wavefront error requirements of the grating. If the wavefront of an echelle grating with dimensions of 400 mm × 500 mm, a blazed order of −36 and a groove density of 79 grooves/mm is expected to be λ/6 (where λ = 632.8 nm), then the peak-to-valley (PV) value of the surface error for the entire grating plane is calculated to be 0.116 μm. The film thickness is related to the grating groove shape, and the maximum metal film thickness required is approximately 10 μm. The length of the diagonal of an entire grating

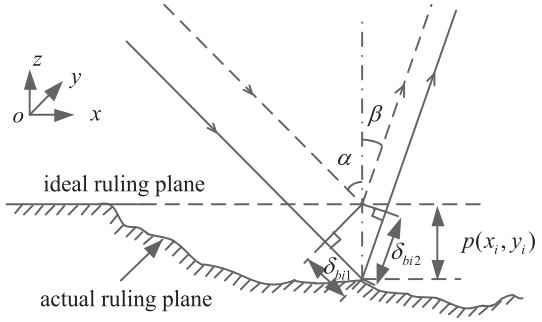

Fig. 1. Schematic of optical path difference due to grating blank surface error.

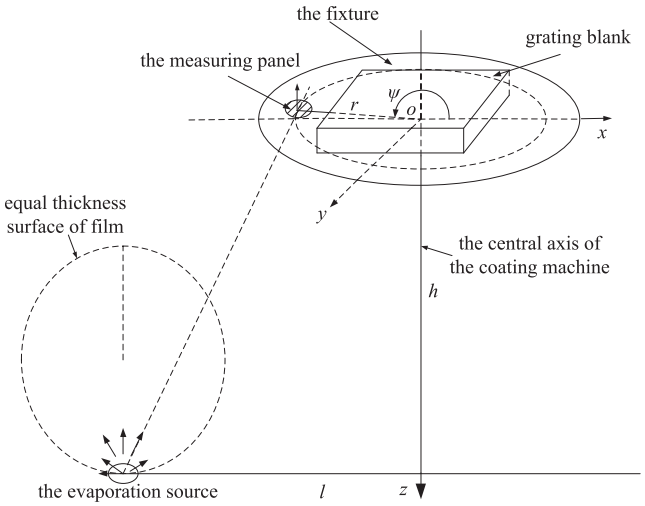

Fig. 2. Schematic of the structure of the coating machine.

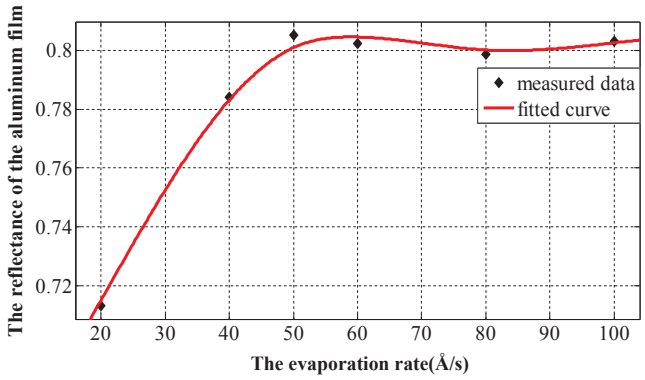

Fig. 3. Relationship between reflectance and evaporation rate of 6-μm-thick aluminum film.

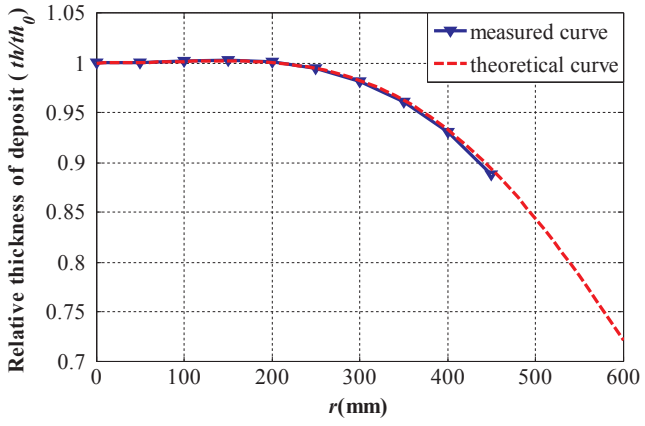

Fig. 4. Measured and theoretical metal film thickness distribution curves used to determine the n value.

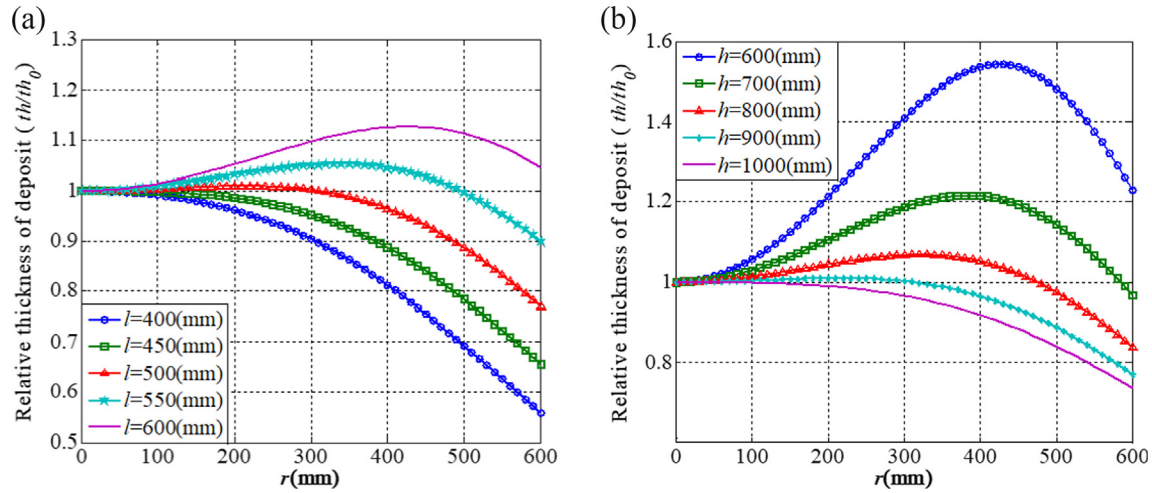

Fig. 5. Theoretical curves of the metal film thickness distribution with respect to h and l. (a) Theoretical film thickness distributions for various l values when h = 900 mm. (b) Theoretical film thickness distributions for various h values when l = 500 mm.

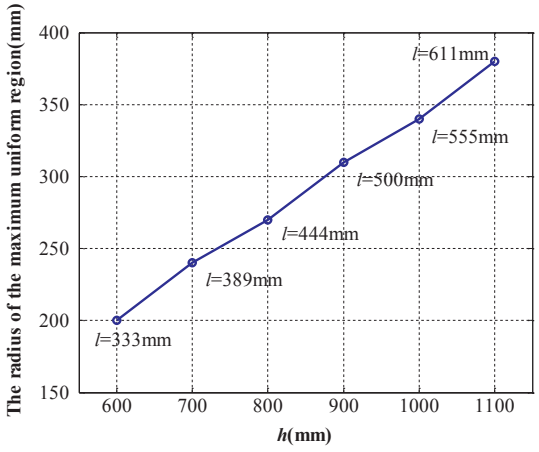

Fig. 6. Maximum radius values corresponding to the optimal l value at various values of h.

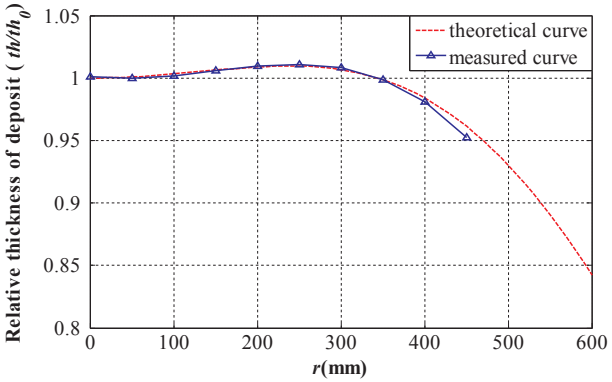

Fig. 7. Measured and theoretical film thickness distribution curves after n, h, and l are determined.

with a ruling area of 400 mm × 500 mm is 641 mm, and the film non-uniformity over the 650 mm diameter range of the coating machine must be less than 1%.

To improve both the efficiency and the thickness uniformity in large-area metal film fabrication, we have adopted an electron-beam evaporation coating device with a rotatable plane fixture. A schematic of the coating machine structure is shown in Fig. 2. The emission characteristics of the electron-beam evaporation source have specific directionality. According to the theory of film deposition and the geometrical relationships of the coating device, the thickness at any point on the rotatable plane fixture can be given by [20,21]:

$$th = \frac{CM}{\pi\rho}\int_0^{\pi}\frac{h^{n+1}}{(h^2 + l^2 + r^2 - 2rl\cdot\cos\psi)^{(n+3)/2}}d\psi \tag{4}$$

where C is a constant, M is the evaporation rate, and ρ is the density of the deposited metal film; h is the vertical distance from the metal evaporation source to the evaporation surface of the fixture, l is the distance from the evaporation source to the central axis of the coating machine, r is the distance from the coating machine axis to the measuring panel axis, and n describes the evaporation characteristic of the electron-beam source.

The film thickness at the center axis of the fixture can then be obtained as follows:

$$th_0 = \frac{CM}{\pi\rho}\int_0^{\pi}\frac{h^{n+1}}{(h^2 + l^2)^{(n+3)/2}}d\psi = \frac{Cmh^{n+1}}{\rho(h^2 + l^2)^{(n+3)/2}} \tag{5}$$

From Eqs. (4) and (5), the ratio of the thickness at the radius to that at the center of the substrate fixture can be calculated as:

$$\frac{th}{th_0} = \frac{\int_0^{\pi}\frac{h^{n+1}}{(h^2+l^2+r^2-2rl\cdot\cos\psi)^{(n+3)/2}}d\psi}{\int_0^{\pi}\frac{h^{n+1}}{(h^2+l^2)^{(n+3)/2}}d\psi} \tag{6}$$

When the grating blank is coated, the ruled grating plane is coplanar with the fixture's evaporation plane, and the geometrical center of the grating blank coincides with the central axis of the coating machine. The grating blank plane to be coated is defined as the xoy plane; the geometric center of this plane is set as the origin o, and the coordinate system shown in Fig. 2 is established. After the grating blank has been coated, the thickness characteristics of the metal film on the blank are given by the following relationship:

$$\begin{cases} x_i = r\cos\psi; \quad y_i = r\sin\psi \\ z_i = \frac{Cm}{\pi\rho}\int_0^{\pi}\frac{h^{n+1}}{(h^2+l^2+r^2-2rl\cdot\cos\psi)^{(n+3)/2}}d\psi, \ (|x| \leqslant a, \ |y| \leqslant b) \end{cases} \tag{7}$$

where a is the groove length, and b is the ruling width perpendicular to the grooves.

Eqs. (3) and (7) can be combined to allow the mathematical model of the relationship between the non-uniformity of the metal film thickness and the grating wavefront error to be written as:

$$\Delta(m) = z(x, y)\cdot(\cos\alpha + \cos\beta_m) \tag{8}$$

where $z(x,y)$ is the surface shape error of the blank caused by the non-

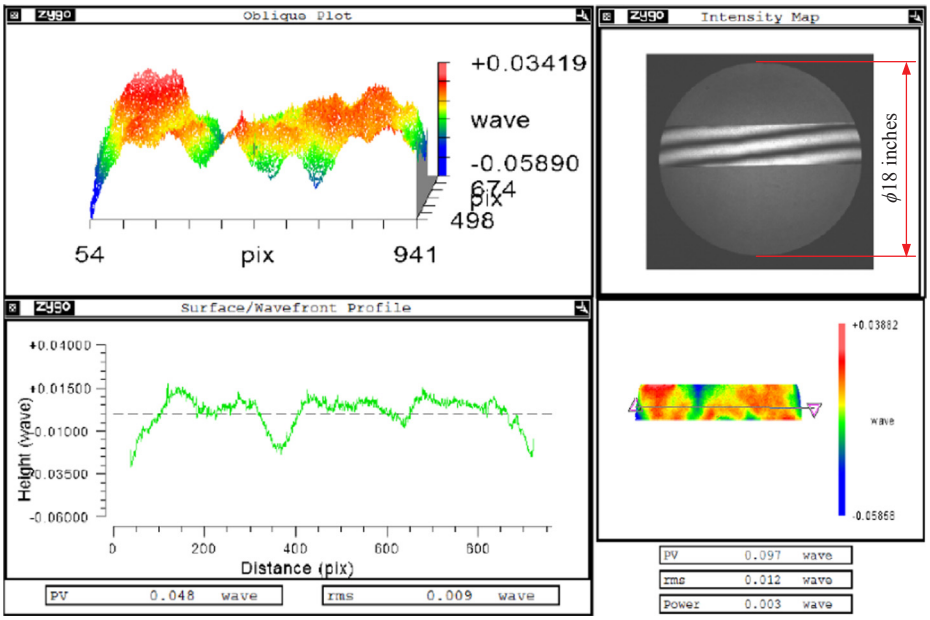

Fig. 8. Surface shape error of the substrate before coating, as measured using a Zygo interferometer.

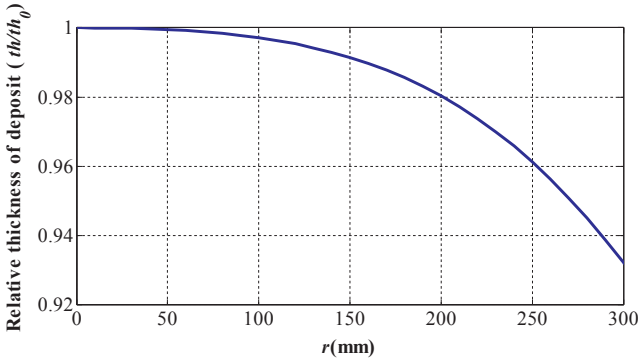

Fig. 9. Theoretical metal film thickness distribution curve when the evaporation rate is 50 Å/s, $h = 800$, and $l = 400$.

uniformity of the metal film thickness and can be calculated using Eq. (7), and β_m is the mth-order diffraction angle and can be calculated using the Eq. (2).

3. Results

3.1. Influence of relevant factors on the metal film thickness

Eq. (6) shows that the thickness distribution of metal film is mainly affected by the variables n, h and l. Factors that affect the value of n include the film evaporation rate, the evaporation source characteristics, and the material to be evaporated. For metal film deposition in the grating fabrication, an electron-beam evaporation coating device is used, the material to be evaporated is pure aluminum, and the value of n is mainly affected by the evaporation rate. The evaporation rate affects not only the thickness uniformity of the aluminum film but also affects the reflectance and determines whether it is easy to form the ideal groove shape. Regardless of the other factors that affect the grating groove shape, grating ruling experiments show that as the reflectivity of the metal film increases, it becomes easier to fabricate the groove shape. Fig. 3 shows the relationship between the reflectance of a 6-μm-thick aluminum film and the film evaporation rate. To express the observed tendency visually, a curve is fitted to the measured data using the smoothing spline in Matlab/Curve Fitting. The reflectance was measured at an angle of 5° between the incident light and the reflected light at using a wavelength of 632.8 nm, and the evaporation rate is measured using quartz-crystal monitors during the aluminum film deposition. Fig. 3 indicates that the reflectance of the aluminum film tends to stabilize as the evaporation rate increases. However, the kinetic energy of the aluminum increases with the increasing evaporation rate, which leads to higher substrate temperatures. High deposition temperatures will contribute to large-size grain growth, which results in increased numbers of internal defects and greater surface roughness [19]. Therefore, the evaporation rate was set at 50 Å/s.

After the evaporation rate is determined, we determine the value of n in Eq. (6) by fitting the measured data. The metal film thickness data along the radius direction of the fixture at $l = 480$ mm and $h = 900$ mm are measured using the atomic profiler; all measured thickness values are then divided by the thickness of the aluminum film at $r = 0$ to obtain the thickness ratios. The least squares fitting method is used to determine the value of n in Eq. (6), and the fitted n value is 4.5 ± 0.113 at 95% confidence level. As shown in Fig. 4, the measured and theoretical metal film thickness distribution curves are basically well matched.

After the value of n is determined, the effects of h and l on the film thickness uniformity are simulated using Eq. (6). Fig. 5(a) shows the effect of the l values on the film thickness distributions along the radius direction when h is a fixed value (900 mm), while Fig. 5(b) shows the metal film thickness distributions along the radius direction for various h values when $l = 500$. Fig. 6 shows that when one of the values of h and l has been determined, the other must have a value such that the region with film non-uniformity of less than 1% has a maximum radius value. Given that adjustment of l is more convenient than adjustment of h, the maximum radius values that correspond to the optimal l value at various values of h are given as shown in Fig. 6. As Fig. 6 illustrates, the radius of the maximum uniform region increases as both l and h increase, but any increases in l and h will lead to requirements for more film materials and longer coating times to deposit films to the same thickness. Taking the time and costs of the coating process and the adjustments to the evaporation source and the fixture into account, we expect the values of l and h to be as small as possible when the requirement for non-uniformity of less than 1% for the 10-μm-thick film over the 650 mm diameter range of the coating machine is met. Therefore, it can be determined from Fig. 6 that the optimum values of h and l are 1000 mm and 550 mm, respectively.

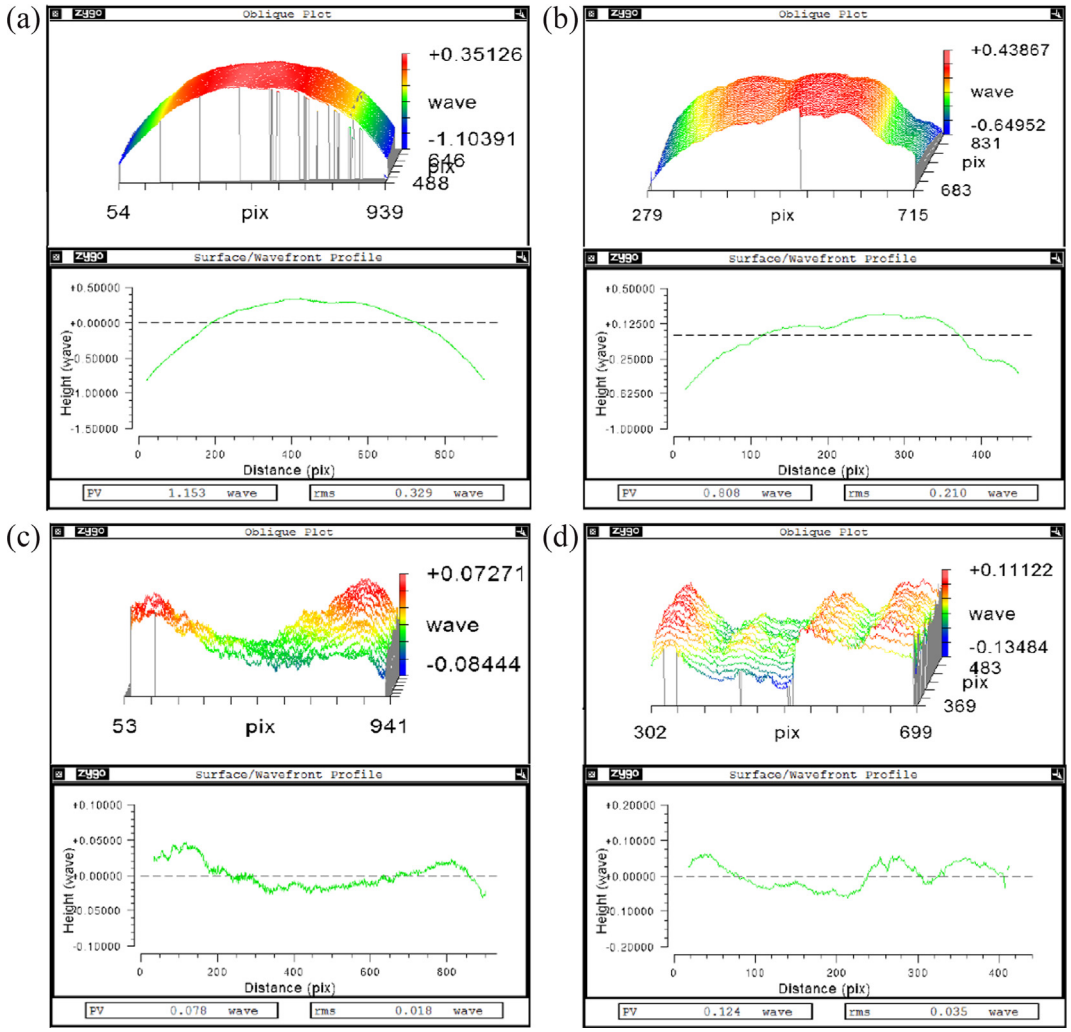

Fig. 10. Wavefront errors of the blank and the grating diffraction order measured using a Zygo interferometer. (a) Surface shape error of the ruled region of the blank measured using the Zygo interferometer before the improvement in the thickness uniformity. (b) Wavefront error of the grating diffraction order measured using the Zygo interferometer before the improvement in the thickness uniformity. (c) Surface shape error of the ruled region of the blank measured using the Zygo interferometer after the improvement in the thickness uniformity. (d) Wavefront error of the grating diffraction order measured using the Zygo interferometer after the improvement in the thickness uniformity.

As shown in Fig. 7, after the values of n, h, and l have been determined, the film thickness distribution curves along the radius direction can be obtained using a combination of theoretical calculations and experimental testing. The results presented here show that the curves that were obtained via these two methods are basically well matched, and the diameter of the region with film non-uniformity of less than 1% is 680 mm, which meets the diameter requirement of 650 mm.

3.2. Effect of metal films non-uniformity on the grating diffraction wavefront

To verify the theory described above, before the film thickness uniformity adjustment, we deposited a 10-μm-thick metal film on a 100 mm × 500 mm × 100 mm grating substrate at an evaporation rate of 50 Å/s, with $h = 800$, and $l = 400$; we then ruled an experimental echelle with dimensions of 75 mm × 450 mm, a blazed order of −35, and a groove density of 79 grooves/mm. After the values of n, l, and h are determined, the requirement for non-uniformity of less than 1% for the 10-μm-thick film over the 650 mm diameter range of the coating machine is met; we also deposited a 10-μm-thick metal film on a 100 mm × 500 mm × 100 mm grating blank, and ruled an experimental echelle with dimensions of 60 mm × 466 mm, a blazed order of −36, and a groove density of 79 grooves/mm.

A Zygo interferogram of the surface shape error of the substrate is shown in Fig. 8. The grating substrate length is 500 mm, and the interferometer aperture size is 18 in. The observed area is limited by the interferometer aperture size. As shown in Fig. 8, the interference fringes observed before coating are very straight, and the PV value of the substrate surface error in the aperture of the interferometer is 0.097 λ (where λ = 632.8 nm). There is no mutation in the unmeasured area and the influence of the substrate surface error on the grating wavefront can be ignored.

Fig. 9 shows the theoretical metal film thickness distribution curve when the evaporation rate is 50 Å/s, $h = 800$, and $l = 400$; the coating thickness non-uniformity over the 18 in range is 3.17%, and the PV values of the wavefront of the grating blank and the grating at the diffraction order (−35th) are calculated using Eq. (8) to be 1.002λ and 0.4853λ (where λ = 632.8 nm), respectively.

Fig. 10 shows the surface error of the grating blank and the diffraction order wavefront error of the grating before and after the improvements in the thickness uniformity. Figs. 9 and 10(a) show that the theoretical profile and the surface/wavefront profile of the grating blank surface error are consistent. The theoretical and measured values

for the grating blank surface error are 1.002λ and 1.153λ, respectively, and the results of the theoretical calculations and the experiments are basically the same.

Comparison of Fig. 10(a) with Fig. 10(b) shows that the surface/wavefront profile curves of the grating blank surface error and the grating are similar, thus indicating that the grating wavefront is mainly affected by the surface errors of the grating blank. However, local feature changes in the surface/wavefront profile curve in Fig. 10(b) are more apparent than those in the curve in Fig. 10(a), and the value of the wavefront of the grating diffraction order exceeds the theoretical value of 0.4853λ, thus indicating that there is another important influencing factor in addition to the surface error of the blank. We use laser interferometers as the position sensor for the grating ruling engine. Changes in the refractive index of the air will cause measurement errors and will thus affect the grating wavefront. We use the wavelength tracker to monitor the ruling environment, in which the ruling engine is located, in real time. By processing the monitoring data, we show that the main reason why the value and the profile of the wavefront of the grating diffraction order in Fig. 10(b) are inconsistent with the corresponding theoretical results is the measurement error caused by the change in the refractive index of the air.

As shown in Fig. 10(c) and (d), the surface/wavefront profiles are not similar to the theoretical profile shown in Fig. 9, thus indicating that the metal film thickness non-uniformity is not the main factor that affects either the surface shape quality of the grating blank or the wavefront quality of the grating. In addition, obtaining the wavefront quality shown in Fig. 10(d) will also require compensation for the groove errors caused by the environment. As shown in Fig. 8, the measurement area on the substrate is limited by the interferometer aperture. The results shown in Fig. 10(d) indicate indirectly that no mutation occurs in the surface error of the substrate within 466 mm.

Comparison of Fig. 10(a) and (b) with Fig. 10(c) and (d) demonstrates that improvement in the metal film thickness uniformity also improves the surface shape quality of the grating blank and the grating diffraction wavefront effectively.

In this work, we assume that the substrate plane is flat to enable study of the effect of non-uniformity of the grating metal film thickness on the surface error of the grating blank and grating diffraction wavefront. In fact, the substrate flatness also affects the grating blank surface error. To reduce the effects of film thickness non-uniformity on the grating blank surface error, in addition to adjustment of coating machine parameters, we can also vary the surface shape of the grating blank before coating. Specifically, the film thickness distribution of the coating machine is first obtained via both theoretical calculations and actual measurements, and the surface shape of the grating blank is then processed into the shape opposite to that of the thickness distribution. Theoretically, there should be no surface error in the grating blank after the coating process, but this is very difficult to achieve in reality. We actually expect the influence of the surface error of the grating blank on the wavefront of an echelle grating with dimensions of 400 mm × 500 mm, a blazed order of −36 and a groove density of 79 grooves/mm to be less than λ/6 (where λ = 632.8 nm) after the coating process.

4. Conclusions

In summary, we have established a mathematical model of the relationship between the thickness non-uniformity of grating metal films and the grating diffraction wavefront error, and we have also analyzed the effects of the relevant factors on the thickness of the metal films through both simulations and experiments. We determined the required evaporation rate and fitted the value of n using the reflectivity of the aluminum film; we then adjusted h and l such that the diameter of the uniformity region with film non-uniformity of less than 1% for a 10-μm-thick aluminum film that is necessary to meet the requirements of a grating with a ruling area of 400 mm × 500 mm is 680 mm. Finally, the ruling experiments have proved that the grating wavefront quality increases with improvement in the film thickness uniformity.

Funding

The work is supported by the Chinese Ministry of National Science and Technology Program (2016YFF0102006, 2016YFF0103304) and the National Natural Science Foundation of China (NSFC) (61605204).

References

[1] J. Song, L.C. Chen, B.J. Li, A fast simulation method of silicon nanophotonic echelle gratings and its applications in the design of on-chio spectrometers, Prog. Electromagn. Res. 141 (2013) 369–382.
[2] S. Engman, P. Lindblom, Blaze characteristics of echelle gratings, Appl. Opt. 21 (23) (1982) 4356–4362.
[3] P. Lindblom, Echelle gratings acting as one, Appl. Opt. 42 (22) (2003) 4549–4559.
[4] D. Nevejans, E. Neefs, E. Van Ransbeeck, S. Berkenbosch, R. Clairquin, L. De Vos, W. Moelans, S. Glorieux, A. Baeke, O. Korablev, I. Vinogradov, Y. Kalinnikov, B. Bach, J.-P. Dubois, E. Villard, Compact high-resolution spaceborne echelle grating spectrometer with acousto-optical tunable filter based order sorting for the infrared domain from 2.2 to 4.3 μm, Appl. Opt. 45 (2006) 5191–5206.
[5] J. Pazder, M. Fletcher, C. Morbey, The optical design of the wide field optical spectrograph for the Thirty Meter Telescope, Proc. SPIE. 6269 (2006) 626932.
[6] K.G. Bach, B.W. Bach Jr., Large-ruled monolithic echelle gratings, Proc. SPIE. 4014 (2000) 118.
[7] C. Yang, X.T. Li, H.L. Yu, H.Z. Yu, J.W. Zhu, S.W. Zhang, J.X. Gao, Bayinheshig, Y.G. Tang, Practical method study on correcting yaw error of 500 mm grating blank carriage in real time, Appl. Opt. 54 (2015) 4084–4088.
[8] H.L. Yu, X.T. Li, J.W. Zhu, H.Z. Yu, X.D. Qi, S.L. Feng, Reducing the line curvature error of mechanically ruled gratings by interferometric control, Appl. Phys. B 117 (2014) 279–286.
[9] C. Yang, H.L. Yu, X.T. Li, J.W. Zhu, H.Z. Yu, Bayinheshig, X.D. Qi, Y.G. Tang, Real-time monitoring of ruling grating resolution by digital wavefront, Appl. Opt. 54 (2015) 492–497.
[10] X.T. Li, H.L. Yu, X.D. Qi, S.L. Feng, J.C. Chu, S.W. Zhang, Jirigalantu, Y.G. Tang, 300 mm ruling engine producing gratings and echelles under interferometric control in China, Appl. Opt. 54 (2015) 1819–1826.
[11] J. Strong, The evaporation process and its application to the aluminizing of large telescope mirrors, Astrophys. J. 83 (5) (1936) 401–423.
[12] A.P. Bradford, G. Hass, J.F. Osantowski, A.R. Toft, Preparation of mirror coatings for the vacuum ultraviolet in a 2-m evaporator, Appl. Opt. 8 (6) (1969) 1183–1189.
[13] M. Schürmann, P.J. Jobst, S. Yulin, T. Feigl, H. Heiße, S. Wilbrandt, O. Stenzel, A. Gebhardt, S. Risse, N. Kaiser, Optical reflector coatings for astronomical applications from EUV to IR, Proc. SPIE 8450 (2012) 84502K.
[14] S. Wilbrandt, O. Stenzel, H. Nakamura, D. Wulff-Molder, A. Duparré, N. Kaiser, Protected and enhanced aluminum mirrors for the VUV, Appl. Opt. 53 (4) (2014) A125–A130.
[15] G.R. Harrison, N. Sturgis, S.P. Davis, Y. Yamada, Interferometric calibration of precision screws and control of ruling machines, J. Opt. Soc. Am. 41 (8) (1951) 495–503.
[16] G.R. Harrison, S.W. Thompson, H. Kazukonis, J.R. Connell, 750-mm ruling machine producing large gratings and echelles, J. Opt. Soc. Am. 62 (1972) 751–756.
[17] Xiaotao Mi, Yu Haili, Yu Hongzhu, Shanwen Zhang, Xiaotian Li, Xuefeng Yao, Xiangdong Qi, Bayanheshig, Qiuhua Wan, Correcting groove error in gratings ruled on a 500-mm ruling machine using interferometric control, Appl. Opt. 56 (21) (2017) 5857–5864.
[18] Haigui Yang, Zizheng Li, Xiaoyi Wang, Zhenfeng Shen, Jinsong Gao, Shanwen Zhang, Radial-quality uniformity investigations of large-area thick Al films, Opt. Eng. 54 (4) (2015) 045106-1-6.
[19] Zizheng Li, Jinsong Gao, Haigui Yang, Tongtong Wang, Xiaoyi Wang, Roughness reduction of large-area High-quality thick Al films for echelle gratings by multi-step deposition method, Optics Express 33 (8) (2015) 23738–23747.
[20] H.A. Macleod, Thin-Film Optical Filters, fourth ed., CRC Press, Boca Raton, 2010 Chap. 13.
[21] J.F. Tang, P.F. Gu, X. Liu, H.F. Li, Modern Optical thin Film Technology, first ed., Zhejiang University Press, Hangzhou, 2007 Chap. 4.